Physics of the Earth and Planetary Interiors 171 (2008) 48–54

Contents lists available at ScienceDirect

Physics of the Earth and Planetary Interiors

journal homepage: www.elsevier.com/locate/pepi

Modeling mantle convection in the spherical annulus

John W. Hernlund [a,*], Paul J. Tackley [b]

[a] University of British Columbia, 6339 Stores Road, Vancouver, BC V6T 1Z4, Canada
[b] Institute for Geophysics, ETH-Zurich, Hönggerberg HPP L13, Schafmattstrasse 30, 8093 Zurich, Canada

ARTICLE INFO

Article history:
Received 1 November 2007
Received in revised form 15 July 2008
Accepted 23 July 2008

Keywords:
Mantle convection
Numerical modeling
Spherical shell
Annulus geometry

ABSTRACT

Most methods for modeling mantle convection in a two-dimensional (2D) circular annular domain suffer from innate shortcomings in their ability to capture several characteristics of the spherical shell geometry of planetary mantles. While methods such as rescaling the inner and outer radius to reduce anomalous effects in a 2D polar cylindrical coordinate system have been introduced and widely implemented, such fixes may have other drawbacks that adversely affect the outcome of some kinds of mantle convection studies. Here we propose a new approach that we term the "spherical annulus," which is a 2D slice that bisects the spherical shell and is quantitatively formulated at the equator of a spherical polar coordinate system after neglecting terms in the governing equations related to variations in latitude. Spherical scaling is retained in this approximation since the Jacobian function remains proportional to the square of the radius. We present example calculations to show that the behavior of convection in the spherical annulus compares favorably against calculations performed in other 2D annular domains when measured relative to those in a fully three-dimensional (3D) spherical shell.

1. Introduction

Although 3D numerical modeling studies of mantle convection continue to become more practical as computing hardware power and software capabilities increase, a survey of the recent literature shows that 2D models are still predominantly employed. It is clear that increased computing power has not yet (and will never have) supplanted the traditional role of 2D studies, which is to push models further in terms of extreme parameter values and raw spatial resolution than is possible in 3D given the same computing capabilities. Many results from 2D studies, because they are at the frontier of resolution and extreme values of parameters, continue to lay the foundation for fundamental new understanding which is usually only modified in second-order ways by subsequent 3D modeling studies. 2D models also serve as an efficient way to conduct exploratory studies which help lay the foundation for deciding how to maximize the efficiency of covering a more sparse parameter space in 3D. Moreover, complex 2D models that required super-computers only a decade ago can now be run efficiently on a standard desktop or laptop computer without the need to employ larger computing facilities.

An important aspect of mantle convection that is difficult to accurately capture in 2D is that it takes place in a curved 3D spherical geometry. 2D studies of mantle convection in a curved domain between an inner and outer boundary at fixed radii (termed an "annulus") are largely restricted to cylindrical/polar or axisymmetric spherical coordinate representations, and the choice between these domains is mostly motivated by the kind of study one is interested in pursuing. Cylindrical models have the advantage that they do not contain inherent boundaries or axes of symmetry, and the full circle can be spanned by the model domain. As van Keken (2001) argued, one of the main problems in cylindrical annular models is that the relative volume of material contained in the inner portion of the domain is larger than in the case of a spherical shell because the areas of the inner and outer boundaries scale as radius rather than the square of radius. His proposed solution is to scale the inner and outer surface areas of the cylinder by altering their relative radii so that it is equal to the area ratio of the spherical shell. In other words, $r_{oc}/r_{ic} = r_{os}^2/r_{is}^2$, where r_{oc} and r_{ic} are the inner and outer radius of the cylinder and r_{os} and r_{is} for the sphere, the uniqueness of which is enforced by equating the shell thickness, $r_{oc} - r_{ic} = r_{os} - r_{is}$. The consequence of applying this scaling is a smaller inner radius, yielding what appears to be a smaller than usual core. This approach is popular, and for many applications this method should satisfactorily mitigate some of the adverse consequences of utilizing cylindrical domains.

Still, problems can occur with a re-scaled inner and outer radius if the subject of investigation is sensitive to changes in the effective aspect ratio of the annulus. For example, the thermal evolution models used by van Keken (2001) to compare the re-scaled

* Corresponding author.
E-mail address: hernlund@gmail.com (J.W. Hernlund).

0031-9201/$ – see front matter © 2008 Elsevier B.V. All rights reserved.
doi:10.1016/j.pepi.2008.07.037

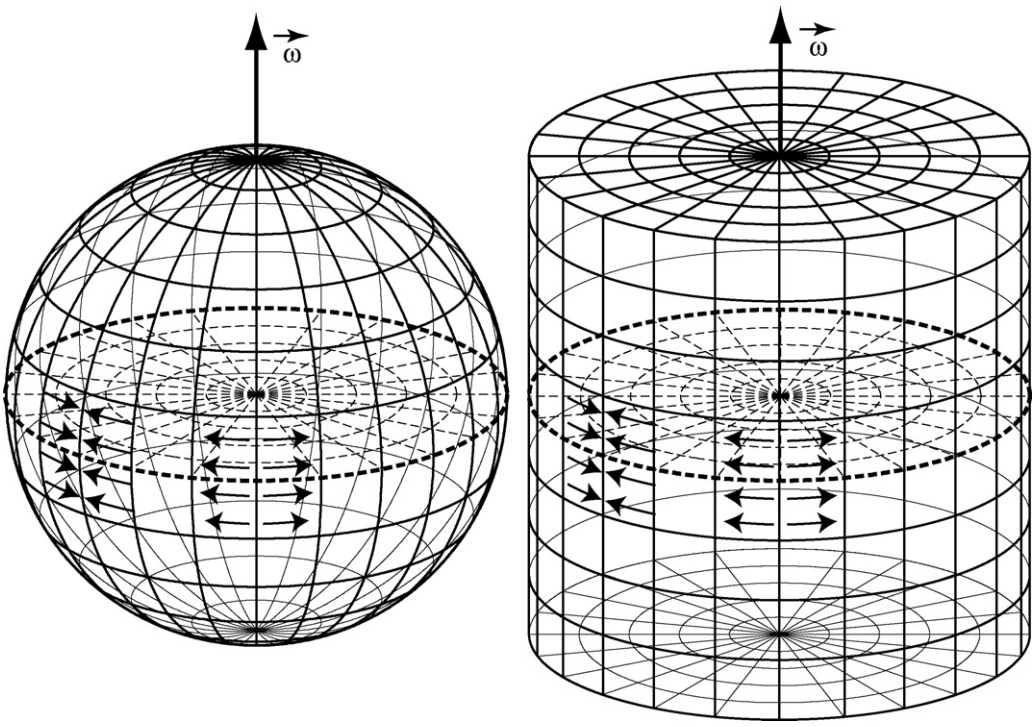

Fig. 1. Comparison between the 2D approximations for rigid body translations on the surface of a sphere (left) and a cylinder (right), with the circular 2D slice of interest indicated by dashed lines. Arrows are shown to indicate a divergent motion such as that along a mid-ocean ridge as well as convergent motion such as a subduction zone setting. In both cases, the angular velocity vector $\vec{\omega}$ describing the 2D lateral motions in the slice is directed along the axes of the coordinate systems if they are taken to be oriented perpendicular to the slice. The primary difference between the two descriptions is that motions on a sphere are projected onto a surface with two degrees of curvature, while a cylinder has only one degree of curvature.

cylindrical annulus with the axi-symmetric spherical case were adjusted to maintain a similar aspect ratio at the top surface. However, when the full annulus (or half annulus) is modeled, there is less effective lateral separation between objects at the base of the rescaled cylindrical shell than is actually the case in a spherical shell. This leads to "crowding" of structures near the inner portion of the annulus around the smaller core. While such crowding does indeed occur in a spherical shell, and is enhanced relative to a cylinder, it is inherently a 3D phenomenon that cannot be projected solely into a single lateral dimension. Examples where such crowding might be problematic are studies of the stability of a dense chemical layer at the base of the mantle (e.g., Nakagawa and Tackley, 2004b) or the effects of phase transitions upon the stability of a lower thermal boundary layer (e.g., Nakagawa and Tackley, 2004a).

While the surface area ratio problem is not present in the spherical axi-symmetric coordinate representation, a bias in the lateral dimension is built into the coordinate basis itself that leads to a variety of anomalous and undesirable effects that render many types of modern mantle convection studies useless. For example, edge effects occur due to a fundamental geometrical bias: the lateral boundary at the poles must be a "reflecting" (zero normal flux, zero tangential stress) impermeable boundary because it is an axis of symmetry. These intrinsic "side walls" affect the pattern and location of upwelling and downwelling flow, an effect that is not present in a real 3D spherical shell. Also problematic is the change in the Jacobian of this coordinate system as material moves along a trajectory of constant radius (such as the inner and outer boundaries): for a non-zero angular velocity, material must undergo pure shear deformation, inducing stresses that are not always an intended part of the model. This occurs because material subjected to an axi-symmetric flow must move along lines of constant longitude, which are further apart at the equator than at higher latitudes. This inability for objects to attain a rigid body lateral motion in the axi-symmetric representation immediately discounts the possibility of attaining plate-like motions at the surface, and would complicate the implementation of stress-dependent rheologies.

We note that there do exist exceptions for cases in which axi-symmetry is quite justified in 2D convection calculations. First, the modeling of approximately axi-symmetric objects alone, such as upwelling plumes, is best captured in axi-symmetric 2D models, and no other 2D coordinate representation can be considered comparable. Second, it is well-established that convective motions in a spherical shell at low Rayleigh numbers (just above critical) do exhibit steady axi-symmetric solutions (Zebib et al., 1980; Schubert and Zebib, 1980). However, as Rayleigh number is increased to moderate values, axi-symmetric solutions are no longer stable (Zebib et al., 1983) and the preferred planform of convective motions becomes tetrahedral or cubic in arrangement (Bercovici et al., 1989; Ratcliff et al., 1995). At Rayleigh numbers similar to those expected in Earth's mantle, the planform is completely three-dimensional and highly time-dependent (Glatzmaier et al., 1990; Bercovici et al., 1992; Schubert et al., 2001). Because the characteristics and stability of axi-symmetric solutions in spherical shell convection have been well and thoroughly investigated, this example is less relevant for modern mantle convection modeling studies.

Here we introduce the "spherical annulus," a simple method for performing mantle convection calculations in an annular domain that does not have the radial scaling problems of the cylindrical polar coordinate system, while at the same time retaining the full periodicity and lateral uniformity of a simple cylindrical polar representation. The coordinate system is obtained geometrically as a bisection of the 3D spherical shell, and the governing equations are obtained by identifying the slice with the equator of a 3D spherical polar coordinate system and eliminating terms that depend on variations in latitude. We present a suite of calculations comparing this and all other available annular methods with those obtained in

a fully 3D convection calculation, and demonstrate that the spherical annulus yields superior results without requiring any re-scaling of the dimensions of the shell.

2. Model formulation

The geometry of the present scenario is summarized schematically in Fig. 1, with the case of a sphere compared to that of a cylinder. A 2D slice is obtained after bisecting the 3D sphere or cylinder with a plane, and in the latter case the normal to the plane is taken parallel to the cylinder's axis so that the domain remains circular in shape. In order to obtain a phenomenological reduction from 3D to 2D, two assumptions are made. First, variations in quantities that may be cast as dependent variables in a direction normal to the planar slice are ignored. Second, a kinematic restriction is needed, and we require the vorticity (defined as $\vec{\omega} = \vec{\nabla} \times \vec{v}$, where $\vec{\nabla}$ is the gradient vector and $\vec{v}$ is the velocity field) of any motions at the location of the slice to be parallel to the direction normal to the slice itself. For material at the slice, this second condition implies that there is no flow in a direction normal to the plane of the slice. These conditions are sufficient to reduce the equations governing mantle convection in the 3D sphere and cylinders to a 2D annular domain.

The essential differences between the equations following the spherical and cylindrical reductions will arise from the fact that in the former case we will neglect terms that measure variations in latitude while in the latter case variations in the axial direction are ignored. Thus in the slice through the sphere, a second degree of curvature is implied in the neglected third dimension that is not carried through in the cylindrical case. The same holds true in the spherical axi-symmetric case, where the slice contains the poles of the spherical coordinate system and variations in longitude are ignored. Although this may be conceptually difficult to understand at first, another way to represent this graphically (Fig. 2) is to present a circular 2D grid and assign it a "virtual" thickness that measures the implied direction of variations that are neglected in the third dimension.

The full 3D governing equations in the infinite Prandtl number approximation for both the sphere and cylinder are listed in Schubert et al. (2001). In the spherical case, we neglect terms containing a derivative with respect to the latitude angle θ and set the latitudinal component of velocity to zero, i.e., $v_\theta = 0$. In the cylindrical case, we neglect terms containing a derivative with respect to the axial direction z, and set the axial component of velocity to zero, i.e., $v_z = 0$. We then find that, for a common radius coordinate r and an angular coordinate ϕ (equivalent to the longitude in the sphere), the reduced governing equations can be expressed together for both cases using a parameter d, such that $d = 1$ for the cylindrical case and $d = 2$ for the spherical case. We denote v_r and v_ϕ as the radial and angular components of velocity, t as the time variable, ρ as the mass density, and g as the acceleration of gravity. Conservation of mass is then given by,

$$\frac{\partial \rho}{\partial t} + \frac{1}{r^d}\frac{\partial}{\partial r}(r^d \rho v_r) + \frac{\partial}{\partial \phi}\left[\rho\left(\frac{v_\phi}{r}\right)\right] = 0. \tag{1}$$

The radial component of the momentum equation is,

$$\frac{1}{r^d}\frac{\partial}{\partial r}(r^d \tau_{rr}) + \frac{1}{r}\frac{\partial \tau_{r\phi}}{\partial \phi} - \frac{\tau_{\phi\phi} + \tau_{\theta\theta}}{r} - \frac{\partial p}{\partial r} - \rho g = 0, \tag{2}$$

while the angular component of momentum is,

$$\frac{1}{r^d}\frac{\partial}{\partial r}(r^d \tau_{r\phi}) + \frac{1}{r}\frac{\partial \tau_{\phi\phi}}{\partial \phi} + \frac{\tau_{r\phi}}{r} - \frac{1}{r}\frac{\partial p}{\partial \phi} = 0. \tag{3}$$

The deviatoric stresses τ are given by,

$$\tau_{rr} = 2\mu\left(\frac{\partial v_r}{\partial r}\right) - \left(k_0 + \frac{2\mu}{3}\right)\left[\frac{1}{r^d}\frac{\partial}{\partial r}(r^d v_r) + \frac{\partial}{\partial \phi}\left(\frac{v_\phi}{r}\right)\right], \tag{4}$$

$$\tau_{\phi\phi} = 2\mu\left[\frac{\partial}{\partial \phi}\left(\frac{v_\phi}{r}\right) + \frac{v_r}{r}\right] - \left(k_0 + \frac{2\mu}{3}\right)\left[\frac{1}{r^d}\frac{\partial}{\partial r}(r^d v_r) + \frac{\partial}{\partial \phi}\left(\frac{v_\phi}{r}\right)\right], \tag{5}$$

$$\tau_{\theta\theta} = (d-1)\frac{2\mu v_r}{r} - (d-1)\left(k_0 + \frac{2\mu}{3}\right)\left[\frac{1}{r^d}\frac{\partial}{\partial r}(r^d v_r) + \frac{\partial}{\partial \phi}\left(\frac{v_\phi}{r}\right)\right], \tag{6}$$

$$\tau_{r\phi} = \mu\left[\frac{1}{r}\frac{\partial v_r}{\partial \phi} + r\frac{\partial}{\partial r}\left(\frac{v_\phi}{r}\right)\right]. \tag{7}$$

where μ is the dynamic viscosity and k_0 is a bulk viscosity that departs from the Stokes approximation. Note that the deviatoric stress $\tau_{\theta\theta}$ must be retained in the spherical reduction, since it contains terms other than those that would arise from latitude variations alone. The energy equation can be found by the same procedure,

$$\frac{\partial e}{\partial t} + v_r\frac{\partial e}{\partial r} + \left(\frac{v_\phi}{r}\right)\frac{\partial e}{\partial \phi} = \frac{1}{r^d}\frac{\partial}{\partial r}\left(r^d K\frac{\partial T}{\partial r}\right) + \frac{1}{r^2}\frac{\partial}{\partial \phi}\left(K\frac{\partial T}{\partial \phi}\right) + H, \tag{8}$$

where e is the energy density, T is the temperature, K is the thermal conductivity,

$$H = H_i + \Phi, \tag{9}$$

is the sum of internal heat production terms H_i and the viscous dissipation function,

$$\begin{aligned}\Phi = {} & 2\mu\left[\left(\frac{\partial v_r}{\partial r}\right)^2 + (d-1)\left(\frac{v_r}{r}\right)^2 + \left(\frac{\partial}{\partial \phi}\left(\frac{v_\phi}{r}\right) + \frac{v_r}{r}\right)^2\right] \\ & + \mu\left[\frac{1}{r}\frac{\partial v_r}{\partial \phi} + r\frac{\partial}{\partial r}\left(\frac{v_\phi}{r}\right)\right]^2 + \left(k_0 + \frac{2\mu}{3}\right) \\ & \times\left[\frac{1}{r^d}\frac{\partial}{\partial r}(r^d v_r) + \frac{\partial}{\partial \phi}\left(\frac{v_\phi}{r}\right)\right]^2\end{aligned} \tag{10}$$

The equations have deliberately been left in a more general form as a reference, although in practice it is usually necessary to make further simplifications, such as referal to a reference state under, e.g., an anelastic or Boussinesq approximation. Boundary conditions are obtained straightforwardly by various restrictions placed on temperature, velocity, and/or the deviatoric stress.

The above equations hold for the cylindrical reduction to 2D when $d = 1$ and the spherical reduction when $d = 2$, and therefore the value of d may be thought of as an effective degree of curvature. Note that the difference between these cases is almost exclusively attributed to a factor of r^d (i.e., r or r^2 for the cylindrical or spherical case) in the divergence terms of the governing equations. This is the well-known Jacobian factor, measuring the variation in a differential element of volume for the coordinate system. In this manner, the effective relative volume of material at the top and bottom of an annular domain in the 2D spherical case retains the same scaling as the full 3D sphere. Note also that, due to this term, further reductions to a one-dimensional radial description yield the same result as the full 3D reduction to 1D, and therefore any reference state

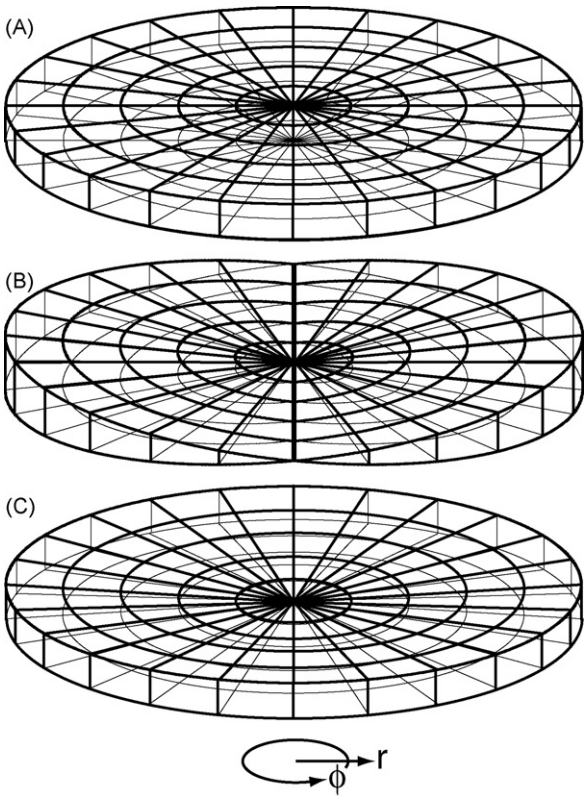

Fig. 2. Illustration of what is meant by the "virtual" thickness J/r of a 2D circular slice through a 3D grid. In the constant thickness case (A), representative of a cylindrical model with effective Jacobian $J = r$, the virtual thickness is constant everywhere. For a variable thickness in the angular direction (B), representative of a spherical axi-symmetric grid with effective Jacobian $J = r^2 \sin\phi$, the virtual thickness depends on the angular location in the grid and the radius. In the variable radial thickness case (C) with effective Jacobian $J = r^2$, the virtual thickness increases with distance from the center of the grid without any angular dependence.

profiles obtained for the spherical 2D reduction will be identical to those applicable in a full 3D sphere. These advantages gained in the 2D spherical reduction are not shared by the cylindrical reduction, hence the need for other remedies such as re-scaling of the inner and outer radii.

3. Example calculations

In order to explore how well a spherical annulus description performs in mantle convection calculations, we have conducted test cases using a modified version of STAG3D (Tackley, 1996), now called STAGYY (Tackley, 2008, this volume) which has also been modified to run cases using the spherical annulus formulation. STAG uses a finite volume formulation to solve the governing equations, however, the spherical annulus may be implemented with all the usual types of modeling technique employed in other 2D geometries. In our test cases, we use a nominal Earth-like outer/inner shell radius ratio of 1.22, and we run several kinds of cases using the spherical annulus, the 2D cylindrical annulus with the scaling of inner radius proposed by van Keken (2001), the 2D spherical axi-symmetric annulus, as well as the full 3D spherical shell using the same code and underlying numerical methodology. We believe the uniformity of resolution and numerical techniques applied in each instance will minimize numerical influences that might otherwise confound a systematic comparison of this kind.

All test cases are for purely thermal convection assuming the Boussinesq approximation. In this case density fluctuations are taken negligibly small in all terms except the buoyancy, the dissipation function is nil, and mass conservation is replaced by the simpler condition $\vec{\nabla} \cdot \vec{v} = 0$. Solutions of the governing equations obtained by integrating forward in time tend to a statistically steady-state whose characteristics depend only on the style of heating, the imposed boundary conditions, and Rayleigh number, which we define as,

$$Ra = \frac{\rho_0 \alpha g \Delta T (r_o - r_i)^3}{\kappa \mu_0}, \tag{11}$$

for bottom-heated convection cases with isothermal inner and outer radii r_i and r_o and,

$$Ra = \frac{\rho_0 \alpha g H_i (r_o - r_i)^5}{K \kappa \mu_0}, \tag{12}$$

for purely internally heated convection cases with an insulating inner radius. Here, ρ_0 is a reference state density, α is the thermal expansivity (assumed constant), ΔT is the super-adiabatic temperature change, κ is the thermal diffusivity (assumed constant), and μ_0 is a reference viscosity. Combinations of $Ra = 10^4$, 10^5, and 10^6, together with purely bottom-heating or internal-heating, and using both isoviscous and temperature-dependent viscosities were run to explore a variety of parameter values and conditions. In the temperature-dependent viscosity cases, the non-dimensionalized viscosity varies by 6 orders of magnitude and is given by,

$$\mu' = \exp[13.8156(0.5 - T')], \tag{13}$$

where T' is the non-dimensional temperature such that $T' = 0$ at $r = r_o$ and in bottom heated cases is $T' = 1$ at $r = r_i$. The reference viscosity μ_0 corresponds to an intermediate non-dimensional value for temperature of $T' = 0.5$.

Typical temperature fields obtained after achieving statistically steady-state conditions in all test cases are summarized in Fig. 3. The basic characteristics of convection in all these instances has already been well-studied, and here we focus on comparative differences in solutions obtained using the different modeling approaches. In Tables 1–4 we list diagnostic output quantities such as RMS velocity v_{RMS} and Nusselt number Nu (the ratio of radial heat transfer relative to that in a purely conductive state at rest), as well as fluctuations in these quantities for time-dependent results. Net rotation is removed in the models, so that this contribution does not appear in v_{RMS}. In general, the spherical annulus consistently yields Nu and v_{RMS} that are closer to values obtained in the full 3D spherical shell than in the cylindrical cases. Indeed, the spherical annulus is often better at obtaining appropriate values than the axi-symmetric case, with the exception of cases where $Ra = 10^4$,

Table 1
Basal heated, isoviscous convection

Ra	Geometry	$\langle Nu \rangle$	$\Delta Nu_{peak-peak}$	$\langle v_{RMS} \rangle$	$\Delta(v_{RMS})_{pk-pk}$
10^4	3D	3.85	Steady	42.3	0
	Spherical annulus	4.18	Steady	37.7	0
	Axi-symmetric	4.01	Steady	41.0	0
	Scaled cylindrical	3.99	Steady	35.6	0
10^5	3D	7.27	0.5	160	11
	Spherical annulus	7.39	0.3	160	14
	Axi-symmetric	7.26	3.2	159	100
	Scaled cylindrical	6.2	2.1	165	90
10^6	3D	15.9	1.3	625	80
	Spherical annulus	14.4	3.4	640	275
	Axi-symmetric	13.7	6.0	520	500
	Scaled cylindrical	14.4	5.5	613	460

$\langle Nu \rangle$ and $\langle v_{RMS} \rangle$ denote time-averaged values once a statistically steady-state is reached. The Δ quantities give the peak-to-peak range of fluctutation during the last part of each run.

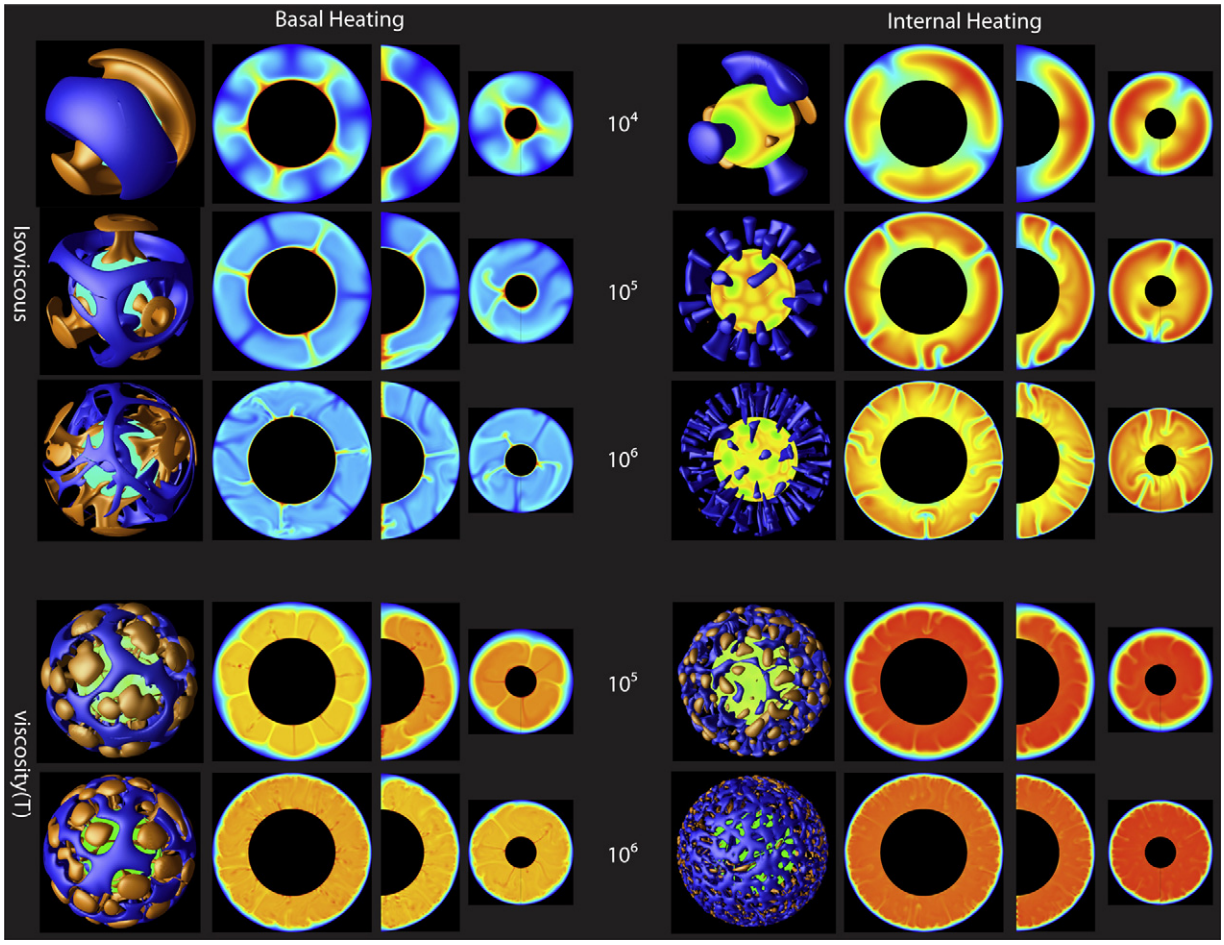

Fig. 3. Comparison of temperature variations for statistically steady-state Boussinesq convection experiments in (from left to right in each group of four) fully 3D spherical, 2D spherical annulus, 2D spherical axi-symmetric, and 2D rescaled cylindrical geometries. Cases are run using the code StagYY (Tackley, 2008, this volume) for the spherical cases and Stag3D for the cylindrical cases. Cases are either completely basally heated (left panel) or completely internally heated with an insulating inner boundary (right panel). The top 3 rows are isoviscous cases, while the bottom 2 rows have temperature-dependent viscosity with 6 orders of magnitude variation between $T' = 0$ and $T' = 1$. The temperature-based Rayleigh number is indicated for each row. The internal heating rate for internally heated cases is set such that they have the same surface heat flux as the basal-heated cases with the same temperature-based Rayleigh number, namely $H = 3.4$ ($Ra = 10^4$ isoviscous), $H = 6.6$ ($Ra = 10^5$ isoviscous), $H = 14.0$ ($Ra = 10^6$ isoviscous), $H = 5.0$ ($Ra = 10^5\mu(T)$), $H = 10.0$ ($Ra = 10^6\mu(T)$); the conventional internal heated Rayleigh number is obtained by the product ($Ra \times H$). The numerical resolution is the same in all geometries, at 32 radial points by 256 points per 2π of azimuth, except for the isoviscous $Ra = 10^6$ cases, which have double this resolution.

where it can be seen that the 3D spherical shell produces roughly axi-symmetric solutions, as expected.

All 2D representations suffer the largest disagreements with the 3D spherical shell when convection is internally heated, and the planform of convection itself becomes highly 3D and is dominated by instability of the upper thermal boundary layer. The best agreement between the 2D models and the 3D shell in internally heated cases occur for $Ra = 10^6$ with temperature-dependent viscosity. In this regime the high viscosity of the cold "lid" plays an important role, limiting convection to small temperature variations at the very bottom of the upper boundary layer that give rise to small scale downwellings. In this scenario, a limiting regime might be reached for large viscosity contrast and Ra where the scaling behavior in

Table 2
Basal heated, temperature-dependent viscosity convection

$Ra_{1/2}$	Geometry	$\langle Nu \rangle$	$\Delta Nu_{\text{peak-peak}}$ [a]	$\langle v_{\text{RMS}} \rangle$	$\Delta(v_{\text{RMS}})_{\text{pk-pk}}$
10^5	3D	6.30	0	405	5
	Spherical annulus	5.71	0.1	463	90
	Axi-symmetric	5.07	0.2	450	210
	Scaled cylindrical	4.97	0.1	495	200
10^6	3D	9.7	0	1804	100
	Spherical annulus	10.1	0.1	1390	780
	Axi-symmetric	10.45	0.1	1370	1040
	Scaled cylindrical	10.4	0.1	1850	1200

$Ra_{1/2}$ is the Rayleigh number defined using the viscosity at $T = 0.5$.
[a] Surface Nu: the CMB Nu fluctuates much more.

Table 3
Internally heated, isoviscous convection

Ra	Geometry	$\langle T \rangle$	$\langle v_{\text{RMS}} \rangle$	$\Delta(v_{\text{RMS}})_{\text{pk-pk}}$
10^4	3D	0.311	23.3	0
	Spherical annulus	0.308	23.5	0
	Axi-symmetric	0.330	25.8	0
	Scaled cylindrical	0.319	22.8	0
10^5	3D	0.322	60.5	7
	Spherical annulus	0.349	78.5	36
	Axi-symmetric	0.357	87.0	65
	Scaled cylindrical	0.384	77.0	75
10^6	3D	0.337	180	10
	Spherical annulus	0.350	265	160
	Axi-symmetric	0.349	270	225
	Scaled cylindrical	0.380	268	350

$\langle T \rangle$ is the volume-averaged temperature.

Table 4
Internally heated, temperature-dependent viscosity convection

$Ra_{1/2}$	Geometry	$\langle T \rangle$	$\langle v_{\mathrm{RMS}} \rangle$	$\Delta(v_{\mathrm{RMS}})_{\mathrm{pk-pk}}$
10^5	3D	0.587	93	4
	Spherical annulus	0.611	135	70
	Axi-symmetric	0.610	142	95
	Scaled cylindrical	0.623	148	90
10^6	3D	0.665	565	65
	Spherical annulus	0.667	575	300
	Axi-symmetric	0.666	560	390
	Scaled cylindrical	0.690	650	430

$Ra_{1/2}$ is the Rayleigh number defined using the viscosity at $T = 0.5$. $\langle T \rangle$ is the volume-averaged temperature.

the spherical annulus and axi-symmetric cases are the same as in 3D. However, the re-scaled cylinder performs poorly in this kind of setting in all cases. In the internally heated cases it is also apparent that v_{RMS} is typically larger in the 2D descriptions than in 3D cases. This is because the strength of 3D flows need not be as great to transfer a given amount of heat given the extra degree of freedom in motions. The 2D cases also show more time-dependence than 3D cases run with the same parameters, although the spherical annulus fares better than the axi-symmetric and re-scaled cylinder in all cases when compared to 3D results.

4. Discussion and concluding remarks

The reduction from 3D to 2D given here for both the spherical and cylindrical cases raises interesting questions regarding how information from a 3D domain may be retained in a more restricted formulation within a 2D slice. Indeed, it appears that any coordinate system that has a circular cross-section for a particular value of one of three variables can be reduced to a 2D section in this manner whenever variations in the neglected third dimension are omitted and motions normal to the plane of the slice are set to be zero. The cylinder and sphere are then only special cases of a more general class of reductions from 3D to 2D. However, information regarding the neglected third dimension is still retained in the 2D equations, particularly with respect to the Jacobian function (see the Appendix A for a more detailed description). The influence of the Jacobian is most relevant in the divergence terms relating to conservation of mass, momentum, and energy, and therefore it is not surprising that the spherical annulus out-performs the cylindrical annulus when comparing to a full 3D spherical shell.

It is interesting to note that there exists a subset of the orthogonal spherical harmonics basis functions that corresponds to a reduction from a 3D sphere to a 2D spherical annulus at the equator. This is the subset for which $(-1)^l = (-1)^m$, where l is the harmonic degree and m is the azimuthal degree. Stated more simply, this restriction calls for m odd when l is odd, or m even when l is even. For these values, derivatives of the spherical harmonic basis functions with respect to latitude vanish at the equator, even though they exhibit variations further away from the equator into the northern and southern hemisphere. The implication is that the restriction to the 2D spherical annulus is compatible with 3D variations in most of the sphere, but of a restricted nature near the equatorial plane. Indeed, by expanding azimuthal variations in quantities at a given depth as a Fourier spectrum, one might in principle obtain estimates of equivalent harmonic degrees that would be obtained in a fully spherical spectrum. However, this will be inherently under-determined because the only information one has regarding harmonic degree l that might correspond to a given m obtained solely by expanding the Fourier components in an equatorial path (or for that matter, any other great circle, so long as the coordinate system is aligned such that it is the equator) is the usual condition $l \geq m$. Nevertheless, this kind of perspective could yield estimates or bounds upon the behavior expected in the full sphere.

For completeness, one needs to interpret what kinds of structure are implied in the third dimension by the 2D plume or other structures obtained in the spherical annular representation. The simplest answer is that these are sheet-like structures, just as with a 2D cylindrical representation, but with a slight additional degree of curvature in the third dimension that causes them to wrap around the sphere into either hemisphere. However, the geometry of the sphere is such that one cannot plausibly imagine making a continuation of the implied sheet-like structures away from the equatorial slice such that they extend and wrap around all the way to the poles of the sphere in either hemisphere. Thus we can only imagine structures being sheet-like in the vicinity of the equatorial plane, and that the structure becomes 3D further into either hemisphere in a way that is completely unconstrained by the variations in the plane itself, as with the spherical harmonic representations mentioned above. Note that this is exactly the same as the usual approximation of 2D geometry at ridges or subduction zones, which are at best only locally 2D and sheet-like into the 3rd dimension in a way that follows the curvature of Earth's surface.

To summarize, we have presented the spherical annulus, a new method for modeling mantle convection in a 2D annular domain in a way that retains the best characteristics of cylindrical coordinates while also saving intrinsic terms in the governing equations related to spherical geometry. The radii of the domain boundaries need not be re-scaled in order to produce spherical behavior. Numerical models of mantle convection show that it is competitive with 2D axi-symmetric models in the manner in which important diagnostic parameters scale with respect to convective vigor and variable viscosity. In fact, in almost every case the spherical annulus performance is superior to that of the 2D axi-symmetric domain, with the exception of isoviscous convection at very low convective vigor. In all cases presented here, the spherical annulus fares better than the re-scaled cylindrical domain. We hope the mantle convection modeling community finds the spherical annulus to be a useful tool in future 2D modeling studies.

Acknowledgments

We thank Stéphane Labrosse and William B. Moore for valuable discussions and feedback. This work was supported by grants from IGPP Los Alamos and the French Ministry of Research, and a CIAR post-doctoral fellowship.

Appendix A

The commonly used equations of motion for mantle convection in the infinite Prandtl number approximation can be written using a generalized Euclidean tensor component representation (e.g., Sokolnikoff, 1951),

$$(\mu \dot{\epsilon}^{ij})_{,j} - G^{ij} p_{,j} + \rho g^i = 0, \tag{14}$$

$$\dot{\epsilon}^{ij} = G^{jk} v^i_{,k} + G^{ik} v^j_{,k} + \lambda G^{ij} v^k_{,k}, \tag{15}$$

$$\rho c_p (\dot{T} + v^i T_{,i}) = (JKG^{ij} T_{,i})_{,j} + H, \tag{16}$$

$$\dot{\rho} + (\rho v^j)_{,j} = 0, \tag{17}$$

which upon expanding covariant derivatives explicitly become:

$$J^{-1} \partial_j (J \mu \dot{\epsilon}^{ij}) + \mu \dot{\epsilon}^{jk} \Gamma^i_{jk} - G^{ij} \partial_j p + \rho g^i = 0, \tag{18}$$

$$\dot{\epsilon}^{ij} = [G^{jk} \partial_k v^i + G^{ik} \partial_k v^j + \lambda G^{ij} J^{-1} \partial_k (J v^k)] + v^l (G^{jk} \Gamma^i_{lk} + G^{ik} \Gamma^j_{lk}), \tag{19}$$

$$\rho c_p (\dot{T} + v^i \partial_i T) = J^{-1} \partial_j (JKG^{ij} \partial_i T) + H, \tag{20}$$

$$\dot{\rho} + J^{-1}\partial_j(J\rho v^j) = 0, \tag{21}$$

where ∂_j is shorthand notation for the partial derivative $\partial/\partial x^j$ with respect to a spatial coordinate x^j (here, a raised index does not imply exponentiation), a comma preceeding an index denotes covariant differentiation with respect to that coordinate index, J is the Jacobian, μ is the viscosity, $\dot{\epsilon}^{ij} (= \dot{\epsilon}^{ji})$ measures the strain-rate, $\Gamma^i_{jk} (= \Gamma^i_{kj})$ are Christoffel symbols of the second kind (i.e., projected derivatives of the basis vectors), $G^{ij} (= G^{ji})$ is the contravariant metric tensor, p is the isotropic pressure, ρ is the density, g^i is the gravitational acceleration, λ is a bulk viscosity factor ($\lambda = k_0/\mu + 2/3$, where k_0 is an excess bulk viscosity), c_p is the specific heat at constant pressure, T is the temperature, K is the isotropic thermal conductivity, H is the internal rate of heat generation (including viscous dissipation), and an over dot on a quantity (e.g., $\dot{T}$) represents a partial derivative with respect to time t only. Note that covariant (lowered indices) or contravariant (raised indices) tensor components are not generally referred to a unit basis, and thus do not represent the "physical components" of the quantities of interest. Repeated indices in the same term, if one is lowered and the other raised, implies summation over the components. Eqs. (18)–(21) are valid in any curvilinear coordinate system, whether orthogonal or non-orthogonal, although they must also be supplemented by an appropriate scalar equation of state $\rho = \rho(p, T)$, rheological model $\mu = \mu(p, T, \ldots)$, and thermal physical models for $K = K(p, T, \ldots)$ and $c_p = c_p(p, T, \ldots)$. Additionally, the form of the equations will depend upon J, G^{ij} and Γ^i_{jk}, which may be obtained from the usual fundamental tensor transformation relations for the particular coordinates to be employed (Sokolnikoff, 1951).

The kind of reduction from 3D to a 2D planar slice proposed in the present manuscript involves retaining the exact same form of Eqs. (14)–(21) as in the full 3D coordinate system by fixing the value of – and neglecting variations with respect to – one of the three coordinate variables. Additionally, we also assume that the velocity and gravity vectors have no component in the neglected dimension (i.e., if the neglected coordinate variable is x^3, then $v_3 = g_3 = 0$) in order that the corresponding neglected component of the momentum equation also vanishes. The Jacobian and remaining components of the metric tensor stay in the governing equations unchanged, even though they retain properties arising from the full 3D coordinate variations. This is the reason why a reduction from the 3D cylinder to a 2D circular slice differs from a circular slice bisecting the 3D sphere: the Jacobian terms in the full sphere are retained in the latter case, which in turn retains intrinsic scaling properties relevant to the spherical geometry and the two degrees of curvature of its boundaries.

References

Bercovici, D., Schubert, G., Glatzmaier, G.A., Zebib, A., 1989. Three dimensional thermal convection in a spherical shell. J. Fluid Mech. 206, 75–104.

Bercovici, D., Schubert, G., Glatzmaier, G.A., 1992. Three dimensional convection of an infinite Prandtl number compressible fluid in a basally heated spherical shell. J. Fluid Mech. 239, 683–719.

Glatzmaier, G.A., Schubert, G., Bercovici, D., 1990. Chaotic, subduction-like downflows in a spherical model of convection in the Earth's mantle. Nature 347, 274–277.

Nakagawa, T., Tackley, P.J., 2004a. Effects of a perovskite-post perovskite phase change near the core–mantle boundary in compressible mantle convection. Geophys. Res. Lett. 31, L16611.

Nakagawa, T., Tackley, P.J., 2004b. Thermo-chemical structure in the mantle arising from a three-component convective system and implications for geochemistry. Phys. Earth Planet. Interiors 146, 125–138.

Ratcliff, J.T., Schubert, G., Zebib, A., 1995. Three-dimensional variable viscosity convection of an infinite Prandtl number Boussinesq fluid in a spherical shell. Geophys. Res. Lett. 22, 2227–2230.

Schubert, G., Zebib, A., 1980. Thermal convection of an internally heated infinite Prandtl number fluid in a spherical shell. Geophys. Astrophys. Fluid Dynam. 15, 65–90.

Schubert, G., Turcotte, D.L., Olson, P., 2001. Mantle Convection in the Earth and Planets, first ed. Cambridge University Press.

Sokolnikoff, I.S., 1951. Tensor Analysis: Theory and Applications. John Wiley and Sons.

Tackley, P.J., 1996. Effects of strongly variable viscosity on three-dimensional compressible convection in planetary mantles. J. Geophys. Res. B 101, 3311–3332.

Tackley, P.J., 2008. Modelling compressible mantle convection with large viscosity contrasts in a three-dimensional spherical shell using the yin-yang grid. Phys. Earth Planet. Interiors 171, 7–18.

van Keken, P.E., 2001. Cylindrical scaling for dynamical cooling models of the earth. Phys. Earth Planet. Interiors 124, 119–130.

Zebib, A., Schubert, G., Straus, J.M., 1980. Infinite Prandtl number thermal convection in a spherical shell. J. Fluid Mech. 97, 257–277.

Zebib, A., Schubert, G., Dein, J.L., Paliwal, R.C., 1983. Character and stability of axisymmetric thermal convection in spheres and spherical shells. Geophys. Astrophys. Fluid Dynam. 23, 1–42.